Supplemental Methods

Animal experiments using Mongolian gerbils

Gastritis was induced in Mongolian gerbils (MGS/Sea; Kyudo, Saga, Japan) by inoculation with *H. pylori* (ATCC43504; ATCC, Manassas, VA) as described (1). After 10 or 50 weeks, gerbils were sacrificed and their stomach was resected.

Methylated DNA binding domain-sequencing (MBD-seq)

DNA methylation in the mouse stomach was analyzed by Methyl-CpG binding domain-based enrichment combined with next-generation sequencing (MBD-seq). Genomic DNA was extracted from gastric epithelial cells of three *H. felis*-infected mice and three mock-treated mice by the standard phenol/chloroform method. From 2 μg of DNA, methylated DNA was enriched using a MethylMiner Methylated DNA Enrichment Kit (Thermo Fisher Scientific). The enriched DNA was dissolved in 20 μl of 1× TE buffer (10 mM Tris-HCl, pH 8.0, 1 mM EDTA), and analyzed by next-generation sequencing.

The enriched and input DNA were end-repaired to generate 3'-dA overhangs, and adapters were ligated to each end using NEBNext Ultra II DNA Library Prep Kit (New England Biolabs). DNA fragments with sizes ranging from 100 to 600 bp were selected by Agencourt AMPure XP (Beckman Coulter) after 15 cycles of PCR amplification, and were sequenced using Illumina HiSeq^{TM}4000 (Illumina) in 150 bp pair-end mode. The obtained sequences were mapped onto the mouse reference genome mm10 using bowtie2 (v2.4.1) (2). To compare the DNA methylation status among multiple samples, DNA methylation levels within the 100-bp bin (region) were calculated using DROMPA3 (v3.7.1) by counting the number of uniquely mapped reads in which all or part of the read was located as described (3). The methylation level in each region was normalized using following formula: $N_{read,t}$

$= U_{read,t} / (N_U / 10^{INT(log10\ Nu)})$ where $N_{read,t}$ was the normalized reads number, $U_{read,t}$ was the uniquely mapped reads number, and N_U was the total uniquely mapped reads number (3). Among all the 100-bp regions, 28,761 regions overlapped with transcription start sites (TSSs) were used for the analysis. Regions with 0.5 or more of normalized methylation levels were defined as methylated.

Hierarchical clustering analysis was conducted using 28,761 regions with TSS using R function hclust (https://cran.r-project.org/).

Bisulfite sequencing using a next generation sequencer (target deep bisulfite sequencing)

The bisulfite conversion was conducted using 1 μg of genomic DNA as described (4). Bisulfite-treated DNA was purified using a Zymo-Spin column I (Zymo Research, Irvine, CA), and DNA was dissolved in 40 μl of 1 x TE buffer. One microliter of bisulfite-treated DNA was amplified using the universal primers listed in Supplemental Table 6, and the PCR product was purified using a Zymo-Spin column I. Using a purified PCR product, a DNA library was prepared, and sequenced using an Ion Proton sequencer (Thermo Fisher Scientific) as described (5). The obtained sequences were converted to CpG methylation statuses using a plug-in for ION Suite based on Bismark (Babraham Bioinformatics, Babraham, UK) as described (6).

Analysis of H3K4me3 and H3K27Ac around the putative promoters of miRNAs

The ChIP-seq data (bigWig data) for H3K4me3 and H3K27Ac in seven human cell lines [GM12878 (GSM733708, GSM733771), H1-hESC (GSM733657, GSM733718), HSMM (GSM733637, GSM733755), HUVEC (GSM733673, GSM733691), K562 (GSM733680, GSM733656), NHEK (GSM733720, GSM733674), and NHLF (GSM733723,

GSM733646)] obtained by ENCODE (7, 8) (https://www.encodeproject.org/) were downloaded using UCSC genome browser (https://genome.ucsc.edu/index.html). The bigWig data were converted into bedGraph using bigWigToBedGraph, and was normalized to reads per million mapped reads. The bedGraph data was displayed in the IGV viewer (9).

Inhibition of NF-kB signaling

293FT cells were seeded (1 x 10^6 cells) on day 0. Then, cells were treated with 0, 3, and 10 μM of Bay 11-7082 (Sigma-Aldrich Japan, Tokyo Japan) on day 1, and were harvested on day 2.

Supplemental Figure legends

Supplemental Figure 1

Activation of NF-κB signaling pathway by chronic inflammation. A) mRNA expression of inflammation-related genes in the human stomach by exposure to chronic inflammation. *NOS2* and *TNF* were up-regulated by exposure to chronic inflammation. Data represent mean ± SD (Welch's *t*-test: *, $p < 0.05$; **, $p < 0.01$). Young: ctrl, n=3, inflamed, n=3. Old: ctrl, n=3, inflamed, n=3. B) Western blotting of the phosphorylated form (Ser536P) of RelA protein in the mouse stomach. C) mRNA expression of the downstream gene of NF-κB signaling pathway in the mouse stomach. *Ccl2* was up-regulated in inflamed mouse stomach. Data represent mean ± SD (Welch's *t*-test: *, $p < 0.05$; **, $p < 0.01$). 40 weeks: ctrl, n=10; inflamed, n=16. 92 weeks: ctrl, n=10; inflamed, n=14.

Supplemental Figure 2

Induction of DNA methylation by exposure to chronic inflammation triggered by *H. felis* infection. A) Unsupervised hierarchical clustering analysis using DNA methylation profiles of 28,761 regions with TSSs. DNA methylation profiles of three inflamed and three control mice were analyzed by MBD-seq. 26,603 regions were commonly unmethylated in three control mice, and 215, 176, and 287 regions (red boxes) were hypermethylated in three inflamed mice. B) Overlap of hypermethylated regions among the three inflamed mice. 138 regions were commonly hypermethylated in two or three mice. C) Representative DNA methylation profiles. DNA methylation levels increased at promoter CpG islands of *Ajap1* in the three inflamed mice. Y-axis represents the read pileup normalized to the total number of reads at a bp position (rpm/bp). D) DNA methylation status of *Ajap1* analyzed by target deep bisulfite sequencing. DNA methylation was induced after a 34-week exposure (40

weeks of age) to chronic inflammation, and its degree became larger after an 86-week exposure (92 weeks of age). E) Overlap of hypomethylated regions among three inflamed mice. 32 regions were commonly hypomethylated in two or three mice.

Supplemental Figure 3

Changes of *Tet* mRNA expression levels in the stomach of Mongolian gerbils by exposure to chronic inflammation analyzed by qRT-PCR. *Tet1* and *Tet3* were mildly repressed after a 10-week exposure to chronic inflammation, but all the three *Tet* genes were repressed after a 50-week exposure. Data represent mean ± SD (Welch's *t*-test: *, $p < 0.05$). 10 weeks: ctrl, n=8; inflamed, n=7. 50 weeks: ctrl, n=9; inflamed, n=10.

Supplemental Figure 4

miRNAs up-regulated by exposure to chronic inflammation. A) miRNA up-regulated by exposure to chronic inflammation in the additional three mice, analyzed using miRNA microarray. B) 36 miRNAs were up-regulated 5-fold or more by exposure to chronic inflammation in the gastric tissues of all the four mice.

Supplemental Figure 5

Prediction of target *TET* genes in human. Six miRNAs, MIR29C, MIR26A, MIR26B, MIR20A, MIR20B, and MIR106B, was predicted to target all the three human *TET* genes.

Supplemental Figure 6

The 5-hmC content in 293FT cells transfected with miRNA mimics. The 5-hmC content was reduced to below-the-detection-limit by MIR29C, MIR26B, and the combination of all

the three miRNAs, and to 58.1% by MIR20A.

Supplemental Figure 7

MIR26B expression levels in the human stomach. Data represent mean ± SD (Welch's *t*-test: *, $p < 0.05$). Young: ctrl, n=3, inflamed, n=3. Old: ctrl, n=3, inflamed, n=3.

Supplemental Figure 8

The correlation between the expression level of MIR26B/MIR29C and that of the three *TET* genes in human gastric tissues (A) and mouse gastric epithelial cells (B). The expression level of MIR26B was negatively correlated with that of *TET3* in both humans and mice.

Supplemental Figure 9

Target sites of MIR26B in the 3'-UTR of *TET3*. A) Schematic illustration of MIR26B target sites within the 3'-UTR of human *TET3*. B) The sequence of the region within the 3'-UTR region of human *TET3* cloned for the luciferase assay.

Supplemental Figure 10

H3K4me3 and H3K27Ac levels in the ENCODE data. Both H3K4me3 and H3K27Ac were enriched around the putative promoter regions of the host genes of MIR26B (*CTDSP1*) (A), MIR20A (*MIR17HG*) (B), and MIR29C (*C1orf132*) (C) in seven cell lines (GM12878, H1-hESC, HSMM, HUVEC, K562, NHEK, and NHLF).

Supplemental Figure 11

RELA binding status around the putative promoter region of MIR29C. RELA binding level at the putative promoter region of MIR29C (*C1orf132*) did not increase by TNF-α treatment.

Supplemental Figure 12

Expression levels of host genes in NUGC-3 cells. The expression level of *MIR17HG* was up-regulated by TNF-α treatment. Data represent mean ± SE (Welch's *t*-test: *, $p < 0.05$).

Supplemental Figure 13

Effects of NF-κB inhibition on expression of the endogenous miRNAs and their host genes. A) Western blotting of the phosphorylated form of RELA protein in 293FT cells treated with a NF-κB inhibitor (BAY 11-7082). B) and C) Effect of BAY 11-7082 treatment on expression levels of host genes (B) and miRNAs (C). Treatment of 293FT cells with BAY 11-7082 repressed expression of *CTDSP1* and *MIR17HG*, but not MIR26B or MIR20A. Data represent mean ± SE (Welch's *t*-test: **, $p < 0.01$).

Supplemental Figure 14

Increased DNMT activity by nitric oxide. Nuclear proteins extracted from gastric cancer cell lines, HSC41 and TMK1, were treated with nitric oxide donors, NOC18 and SNAP, and DNMT activity was measured. DNMT activity was enhanced 3.3- to 4.8-fold by exposure to NOC18 and 1.4- to 1.5-fold by SNAP. NO, treatment with NOC18. Data represent mean ± SE.

Supplemental Figure 15

Effect of nitric oxide on expression levels of the *TET* genes and MIR26B. A) Effect of nitric oxide on expression levels of *TET* genes. Expression levels of *TET1*, *TET2*, and *TET3* were not repressed in two gastric cancer cell lines (TMK1 and HSC41) treated with NOC18. B) Effect of nitric oxide on expression levels of MIR26B. Expression levels of MIR26B were not up-regulated by treatment with nitric oxide. Data represent mean ± SE (Welch's *t*-test: *, $p < 0.05$).

Supplemental Figure 16

Knockdown of *TET3* by three different shRNAs in 293FT cells. Reduction of expression levels of *TET3* was confirmed by qRT-PCR. Data represent mean ± SE (Welch's *t*-test: **, $p < 0.01$).

Supplemental Figure 17

Synergistic effect of a combination of *TET3* repression and NOC18 treatment in two more independent cultures of 293FT cells using two more shRNAs. The synergistic effect of the combination observed in one biological replicate (Figure 4) was precisely replicated in two more cultures. 6,021 (27.9-65.3%) and 27,029 blocks (36.7-59.2%) were commonly methylated by the combination at 4 and 10 weeks, respectively.

Supplemental Figure 18

Knockdown of *TET3* by a shRNA in HSC60 cells. Reduction of an expression level of *TET3* was confirmed by qRT-PCR. Data represent mean ± SE.

Supplemental references

1. Niwa T, Tsukamoto T, Toyoda T, Mori A, Tanaka H, Maekita T, et al. Inflammatory processes triggered by *Helicobacter pylori* infection cause aberrant DNA methylation in gastric epithelial cells. *Cancer Res.* 2010;70(4):1430-40.
2. Langmead B, and Salzberg SL. Fast gapped-read alignment with Bowtie 2. *Nature methods.* 2012;9(4):357-9.
3. Jadhav RR, Ye Z, Huang RL, Liu J, Hsu PY, Huang YW, et al. Genome-wide DNA methylation analysis reveals estrogen-mediated epigenetic repression of metallothionein-1 gene cluster in breast cancer. *Clin Epigenetics.* 2015;7:13.
4. Takeshima H, Yamashita S, Shimazu T, Niwa T, and Ushijima T. The presence of RNA polymerase II, active or stalled, predicts epigenetic fate of promoter CpG islands. *Genome Res.* 2009;19(11):1974-82.
5. Takeshima H, Niwa T, Toyoda T, Wakabayashi M, Yamashita S, and Ushijima T. Degree of methylation burden is determined by the exposure period to carcinogenic factors. *Cancer Sci.* 2017;108(3):316-21.
6. Yoshida S, Yamashita S, Niwa T, Mori A, Ito S, Ichinose M, et al. Epigenetic inactivation of FAT4 contributes to gastric field cancerization. *Gastric Cancer.* 2017;20(1):136-45.
7. Consortium EP. An integrated encyclopedia of DNA elements in the human genome. *Nature.* 2012;489(7414):57-74.
8. Davis CA, Hitz BC, Sloan CA, Chan ET, Davidson JM, Gabdank I, et al. The Encyclopedia of DNA elements (ENCODE): data portal update. *Nucleic Acids Res.* 2018;46(D1):D794-d801.
9. Robinson JT, Thorvaldsdottir H, Winckler W, Guttman M, Lander ES, Getz G, et al. Integrative genomics viewer. *Nat Biotechnol.* 2011;29(1):24-6.

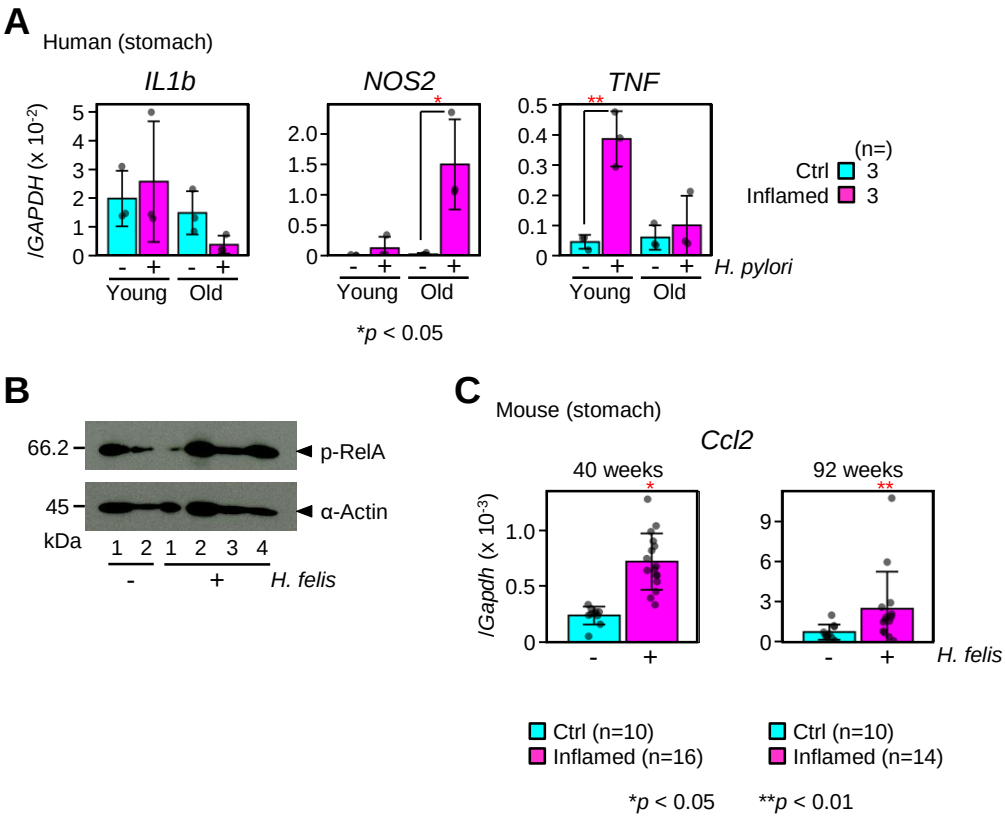

Supplemental Figure 1

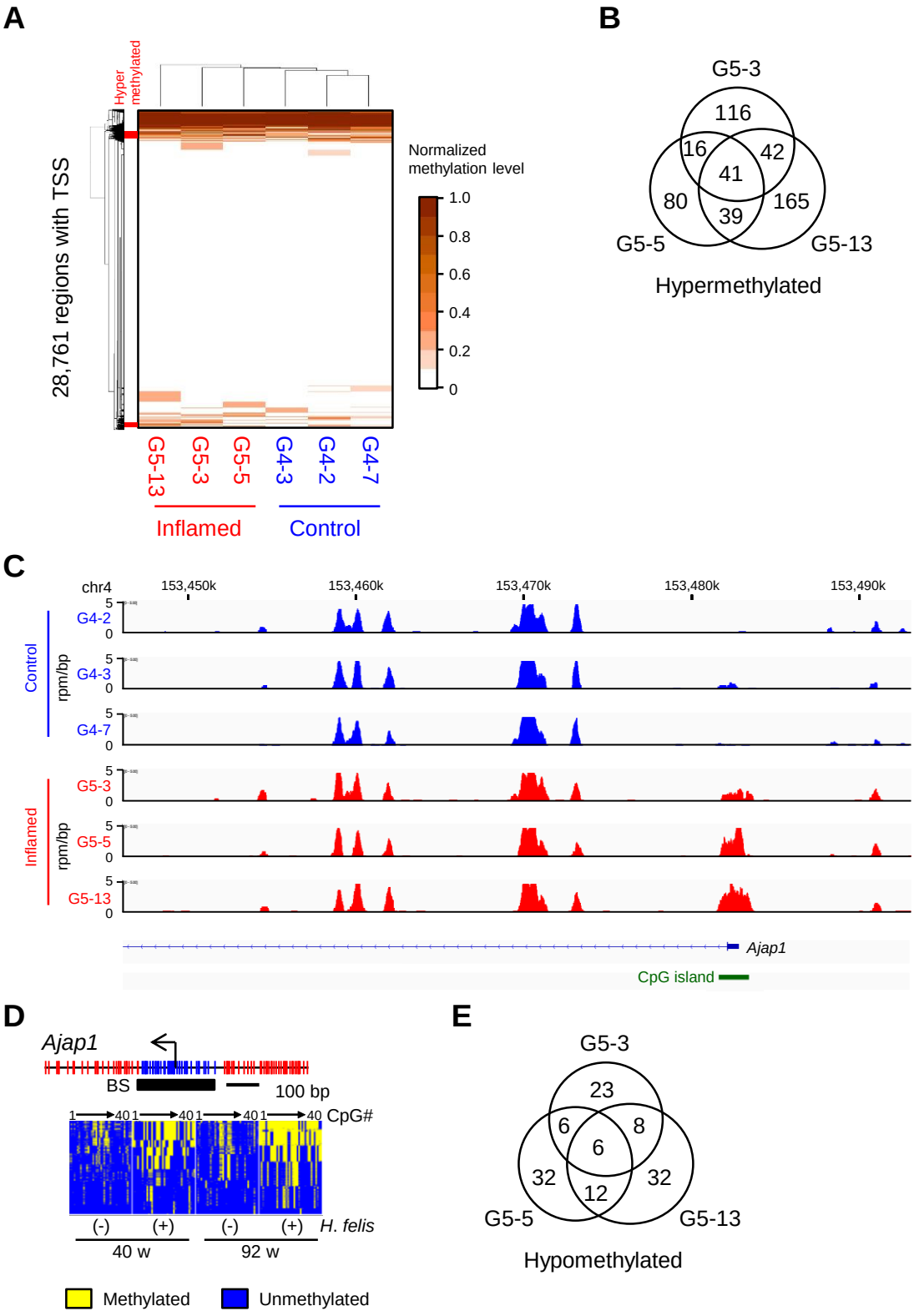

Supplemental Figure 2

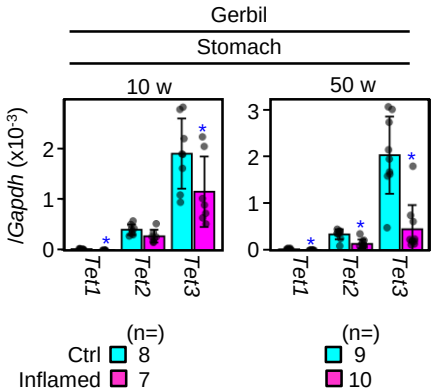

Supplemental Figure 3

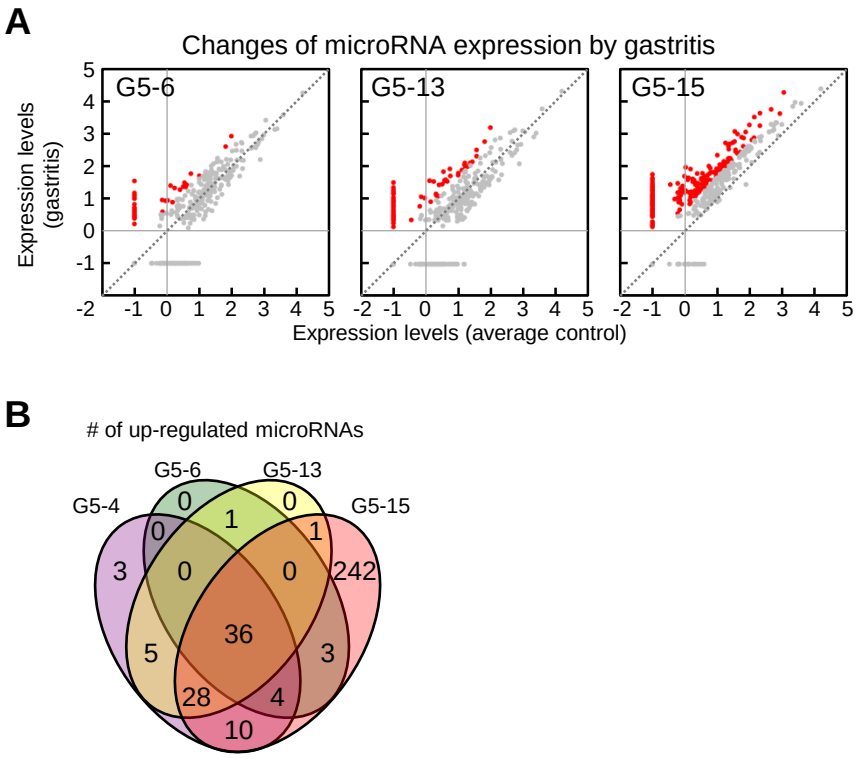

Supplemental Figure 4

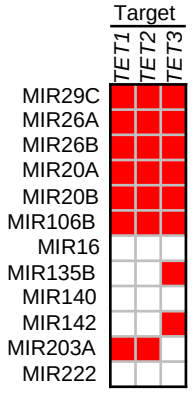

Supplemental Figure 5

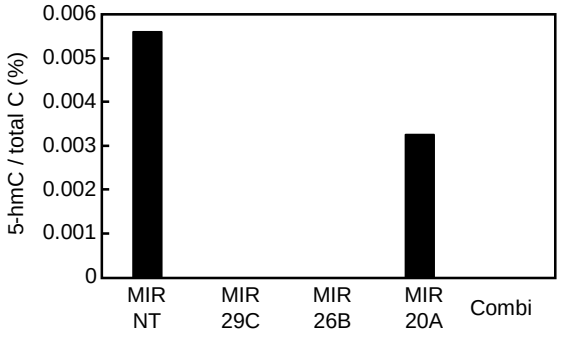

Supplemental Figure 6

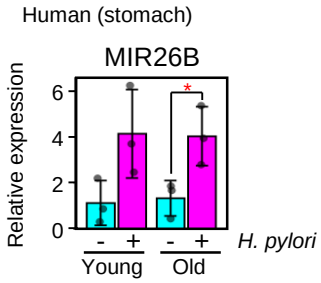

Supplemental Figure 7

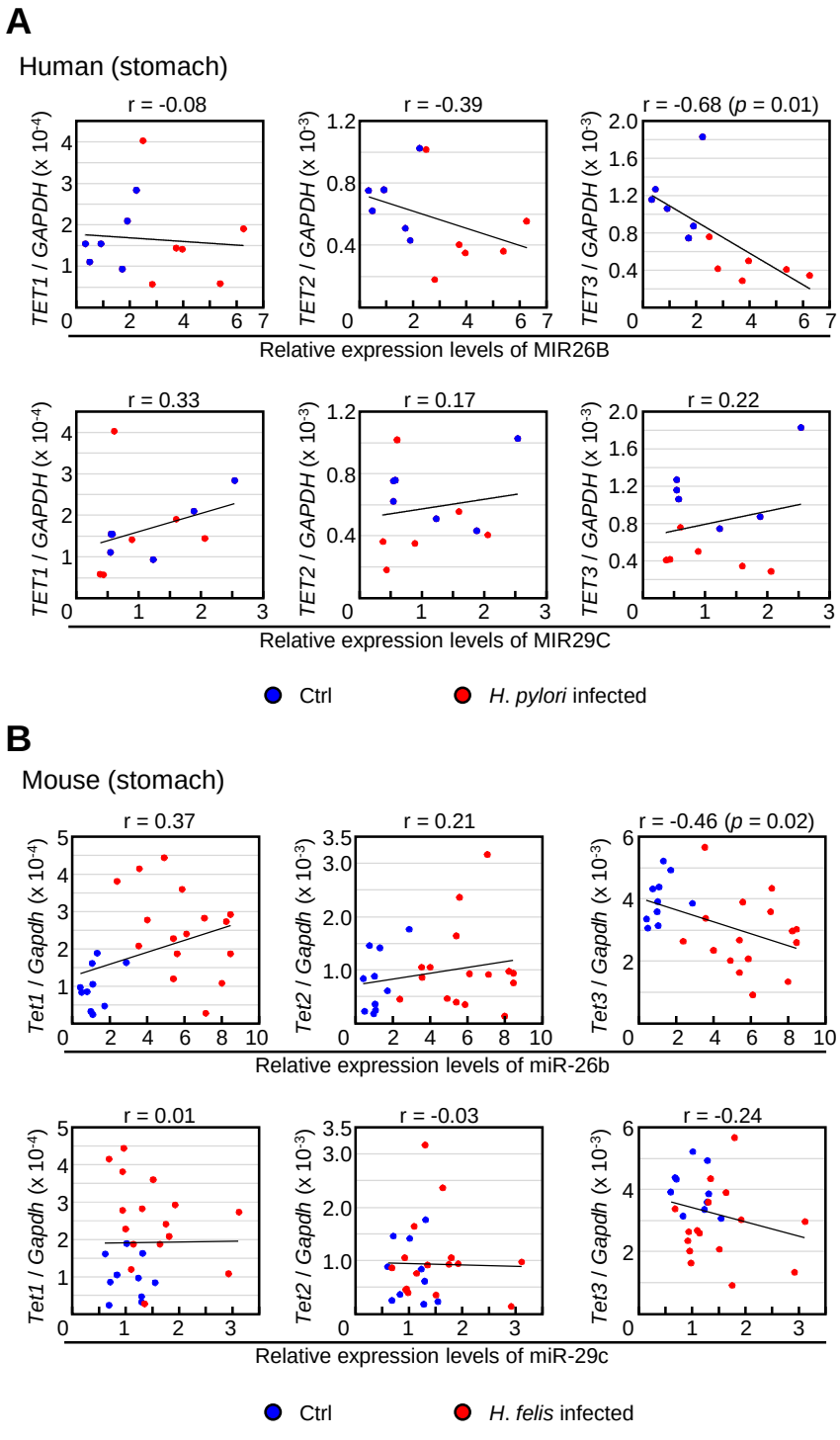

Supplemental Figure 8

A

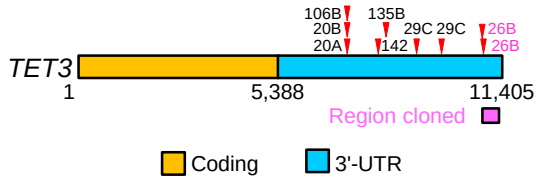

B

Cloned sequence containing MIR26B target sites

```
gggcaggtcg tataatggca tattaataca ttagacttaa tctagaaccc
ctgtagcttt ttgatgtgtt ttatttctta tctctttgaa ttcctgtttg
gttacttggc ttccaatgga ggtgaactta acaaccatac ttgaatattc
cgtcttgact ttgtaaactg tggctacttg aaatgaagtt tatctggggt
tgatggatga atggtagatt tttgcaatgt ctcaaggcaa taggatgtgt
attaaactgt agatattctt agtacagtaa atttatgctg ataattttat
tttgtataat ttttaccttt ttgttaatat tttttccttc cactttattg
gtttgcctcc tgagctaccc ctccttaccc tcccttctcc ctcagtgttt
cagtaaattt aatttagggt gcctagaaat tgcaagtat
```

MIR26B target sites

Supplemental Figure 9

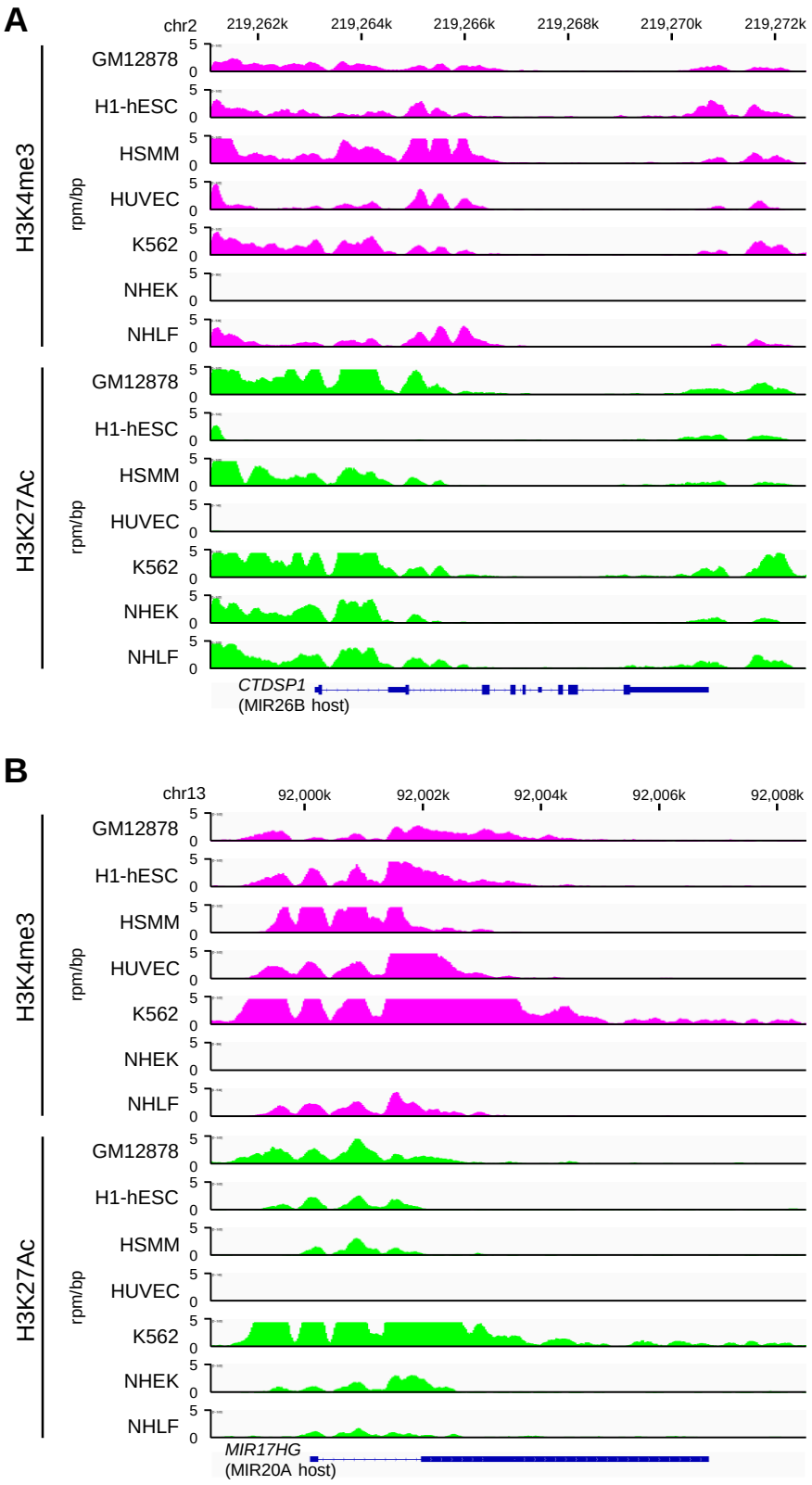

Supplemental Figure 10

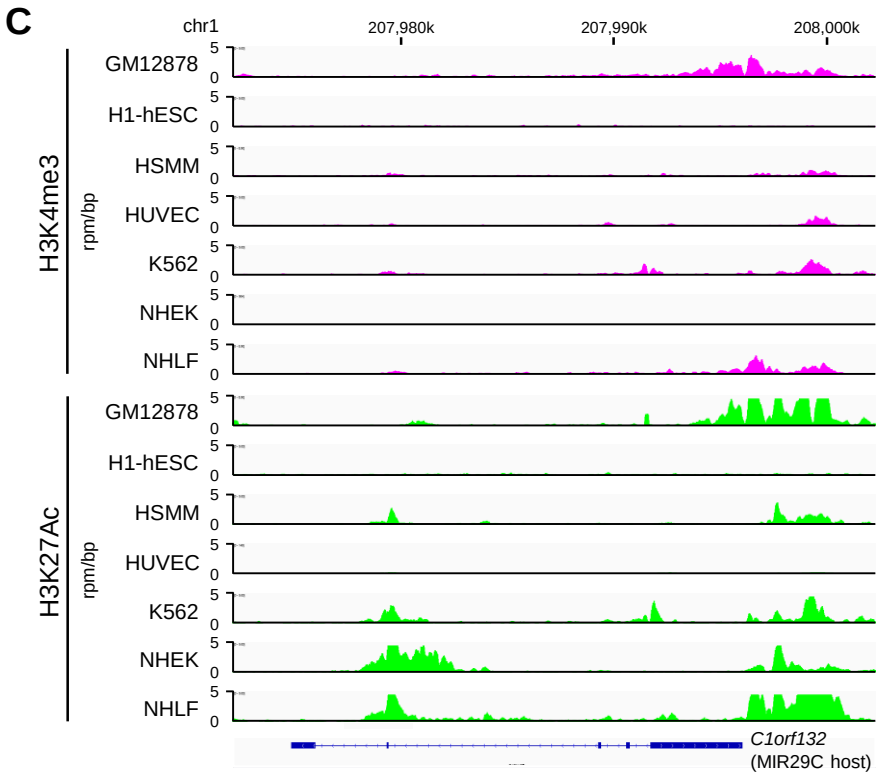

Supplemental Figure 10 (continued)

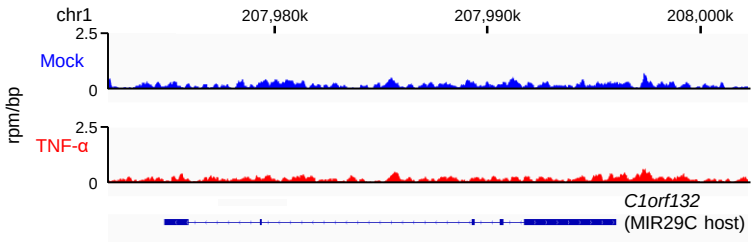

Supplemental Figure 11

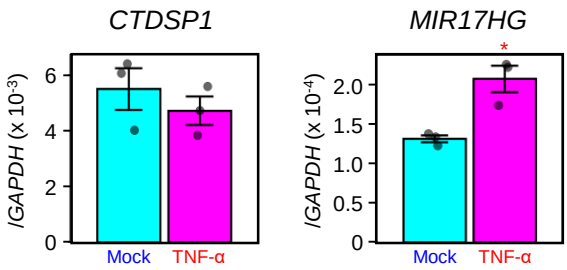

Supplemental Figure 12

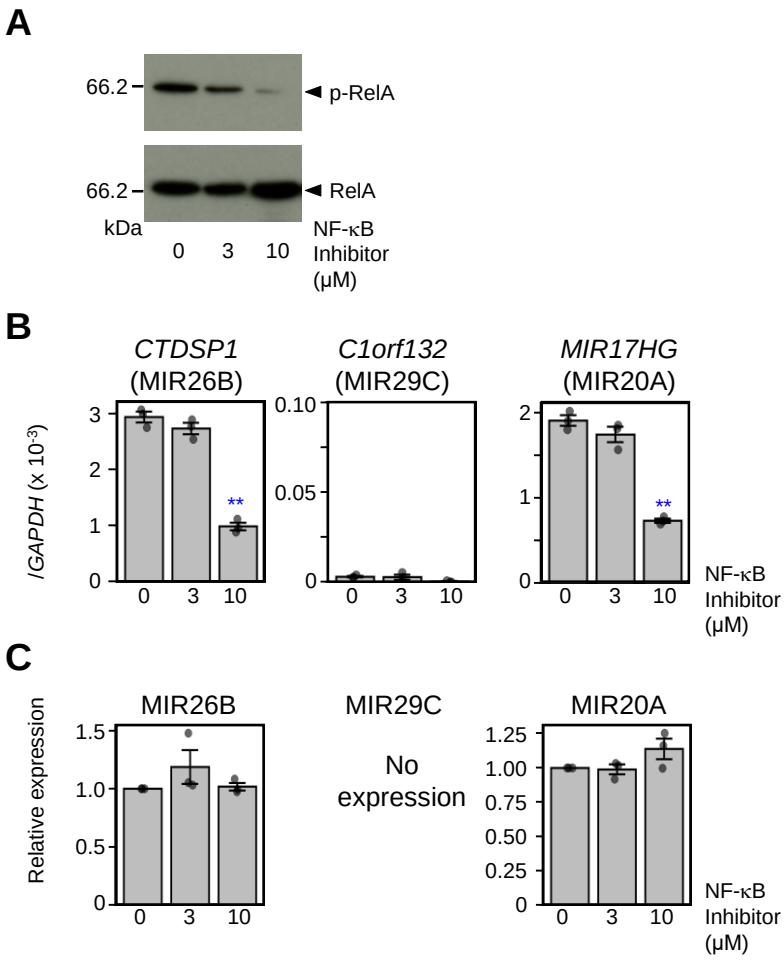

Supplemental Figure 13

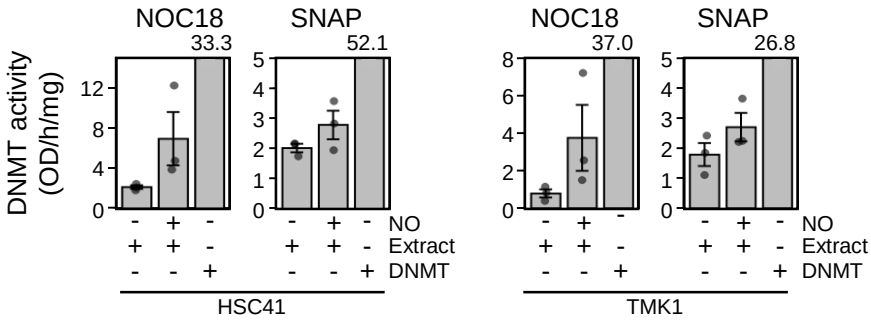

Supplemental Figure 14

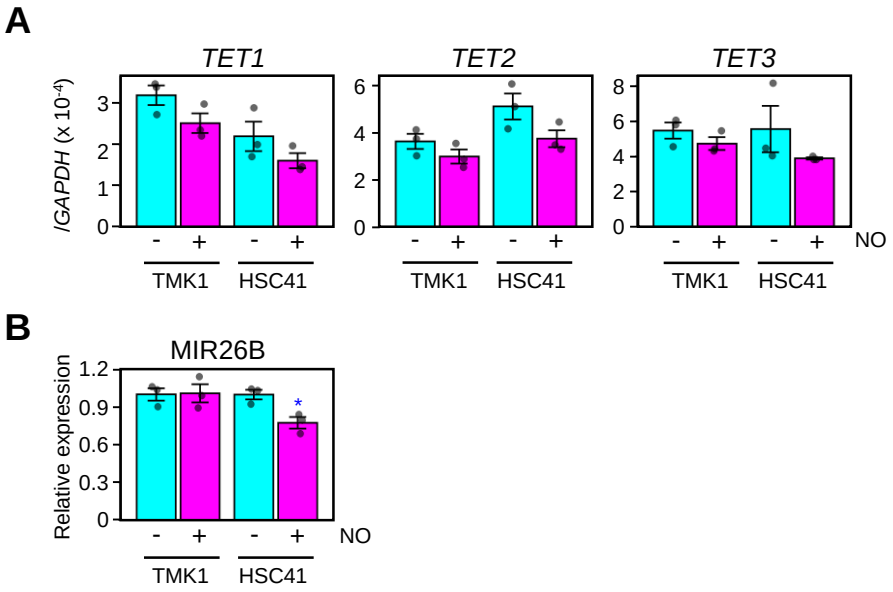

Supplemental Figure 15

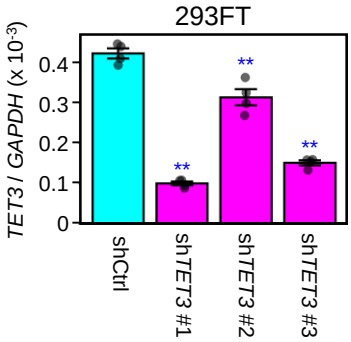

Supplemental Figure 16

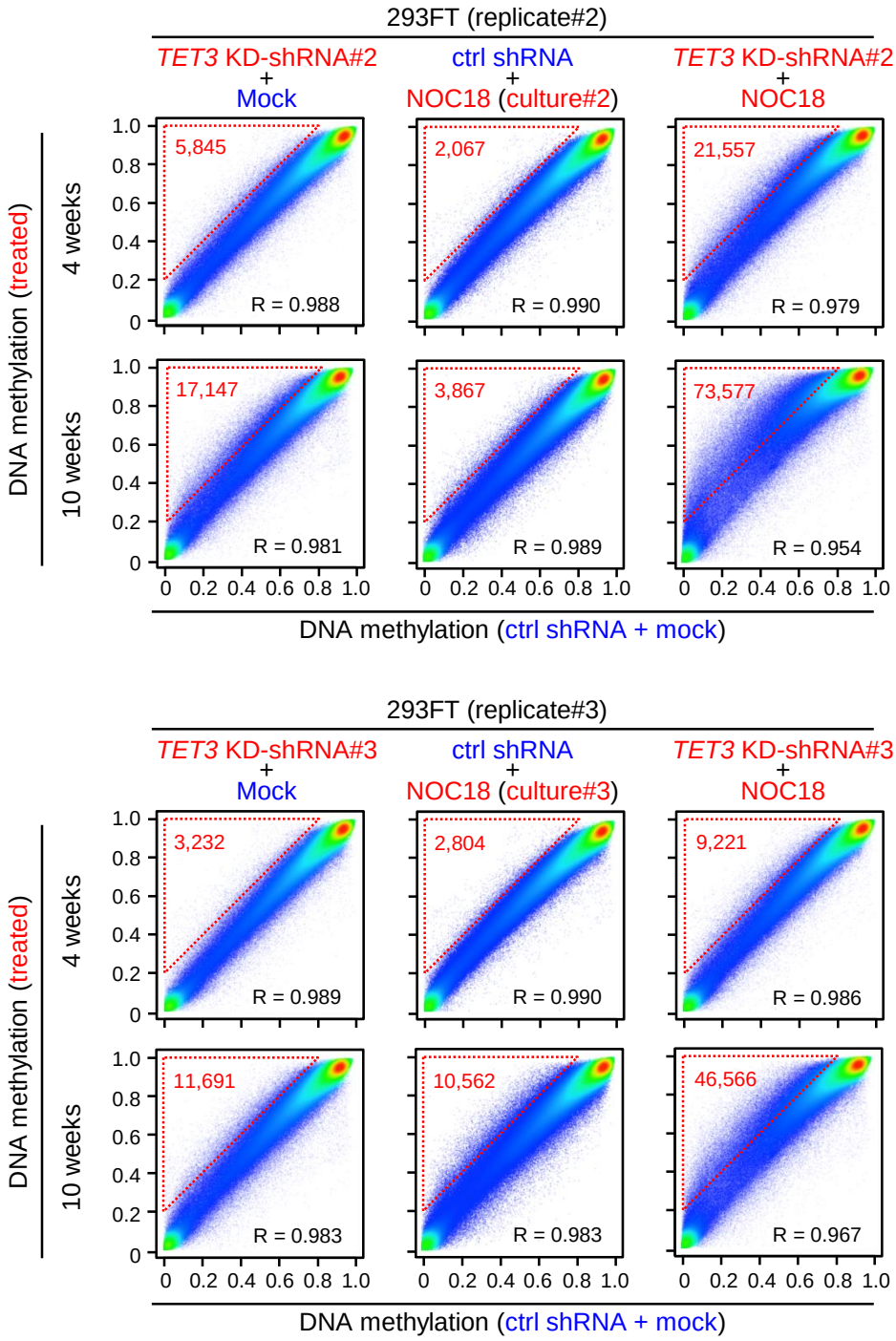

Supplemental Figure 17

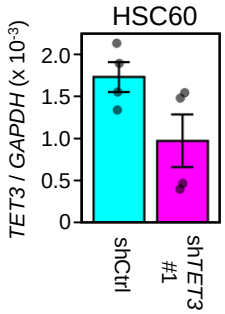

Supplemental Figure 18